Innovative: International Multi-disciplinary Journal of Applied Technology
(ISSN 2995-486X) VOLUME 04 ISSUE 10, 2026

IMPROVED TECHNOLOGY FOR PREPARING PA-6 FILLED USING IRON(II) DIACETATE AND ITS TRIBOLOGICAL PROPERTIES

Qurbonov Mahmudjon Xusanboy o'g'li
Senior Lecturer, Department of Physics, Namangan State University
Email: maxdil9093@gmail.com, ORCID: 0009-0001-8109-8702

Abstract:
A PA-6 filling route was developed through thermal conversion of $Fe(CH_3COO)_2$ in an oil medium at 230–250 °C. Staged dosing, mixing and rapid cooling were integrated with compositional and spectral control. PA-55 contained 8.15 wt.% Fe_2O_3 equivalent and retained its amide I band at 1643.85 cm^{-1}. Comparative tribological analysis of PA-6/Fe gave linear wear of 97 μm/km in water versus 118 μm/km for bronze; in I-50 oil at 2 MPa, the bronze-to-composite wear ratio was 9.77. Composition selection was linked to the wear mechanism.

Keywords: polyamide 6, iron(II) diacetate, thermal conversion, interfacial interaction, friction, wear, oil medium

Introduction

Polyamide 6 is used in guides, bushings and transmission components because it combines processability with the ability to operate against a metallic counterface. During sliding, the condition of its surface layer depends on matrix deformation, heat generation and polymer transfer to the opposing surface. Filler control changes these processes through composition, interfacial contact and the distribution of the solid component[1].

For iron-containing PA-6, the sequence in which the filler forms is significant. Conversion of a molecular precursor directly in the polymer medium connects the emergence of inorganic centres with their contact with macromolecules. We therefore consider temperature, dosing, mixing and cooling as related operations that determine the final composition and the condition of the amide groups [2].

The aim of this work is to substantiate an improved route for preparing filled PA-6 using $Fe(CH_3COO)_2$ and to connect the processing operations with composition, spectral characteristics and comparative friction and wear indicators for PA-6/Fe.

A. Dey and co-workers demonstrated that the products of iron(II) acetate conversion depend on the thermal treatment protocol[3]. S. Musić and co-workers linked the thermal transformations of iron acetates to oxide formation[4]. These studies support control of the

precursor's thermal history.

R. Gupta and co-workers established that the surface condition of iron oxide particles affects their distribution and the properties of PA-6 [5]. The findings of L. Li and G. Yang on hydrogen bonding in polyamide provide a basis for analysing interfacial interactions [6]. We apply this approach when comparing the amide I–III bands.

Materials and Methods

Our previous research established a series of ten samples: the PA-6 reference coded PA-52 and nine composites coded PA-54, PA-55, PA-70B, PA-71, PA-72 and Y-1–Y-4. These codes identify samples. $Fe(CH_3COO)_2$ served as the iron-containing precursor, and its thermal conversion was carried out in plasticised PA-6.

Composition was determined with a Rigaku NEX CG energy-dispersive X-ray fluorescence spectrometer. The Fe_2O_3-equivalent mass fraction was used for processing comparisons. It expresses total iron on a common stoichiometric scale. The calculated matrix fraction was obtained by subtracting the sum of the identified oxide-equivalent components from 100%.

Infrared spectra were obtained with a Shimadzu IRAffinity-1 instrument. The N-H, CH_2 and amide I–III band positions were compared after identical baseline processing. Reflectance spectra were recorded with a Shimadzu UV-2600 over 220–1400 nm, using a 1 nm data interval and a 2 nm spectral slit. Band positions and minimum reflectance were used as diagnostic characteristics of the product.

The tribological part comprised our comparative analysis of the PA-6/Fe series compiled in the preceding study. The water series concerns a composition containing 15 wt.% Fe; the oil series compares PA-6/Fe with OTsS-5-5-5 bronze. Each series retained its own medium and measurement units. The friction coefficient and linear wear intensity were expressed as:

$$\mu = F_t/F_n; \quad I_h \{Citation\} = \Delta h/L. \qquad (1)$$

Here F_t and F_n are tangential and normal forces, Δh is wear depth and L is sliding distance. Linear wear intensity is reported in μm/km. The methodological description of contact uses the load, speed, distance and environment parameters identified in ASTM G99-23.

Results

Processing sequence for composite preparation

We combined polymer preparation, precursor conversion and product isolation into a sequential process. PA-6 is brought to a homogeneous plasticised state in a high-boiling oil medium under pressure. $Fe(CH_3COO)_2$ is introduced after the temperature has stabilised. Table 1 presents the principal processing conditions [7].

Table 1. Operations of the improved preparation route

Operation	Conditions	Purpose
PA-6 preparation	70–85 °C	Moisture removal to constant mass
Plasticisation	230–250 °C	Formation of a homogeneous polymer mass
Precursor dosing	3–5 portions	Distribution of the precursor within the matrix
Mixing	200–600 min^{-1}; 10–30 min	Formation and distribution of iron-containing centres

Operation	Conditions	Purpose
Cooling	Rapid passage through 250–80 °C	Preservation of the formed material state
Washing and drying	Cleaning; 70–80 °C	Oil removal and mass stabilisation

Staged addition reduces local precursor concentration. Mixing distributes the emerging centres throughout PA-6, while rapid cooling shortens the time available for their diffusional growth. The processing advantage of this sequence lies in combining formation of the iron-containing component with its contact with the polymer.

The oil acts as a heat-transfer medium and reduces adhesion of the polymer mass to the reactor walls. Washing uses a medium that preserves PA-6, followed by drying to stable mass. During dosing, temperature is maintained within ±2 °C; stabilisation of mixer torque is used as an operational indicator of the condition of the mass [8].

The formulation was calculated from the balance of iron atoms. The theoretical Fe_2O_3-equivalent yield from anhydrous $Fe(CH_3COO)_2$ is given by the molar-mass ratio:

$$q = M(Fe_2O_3)/[2M(Fe(CH_3COO)_2)] = 0.459047. \quad (2)$$

For 100 g of PA-55 product containing 8.15 g Fe_2O_3 equivalent, the calculated anhydrous precursor requirement is 17.754 g. For $Fe(CH_3COO)_2 \cdot 4H_2O$, the yield is 0.324576 g/g and the corresponding requirement is 25.110 g. Both quantities are stoichiometric calculations for complete conversion and retention of the iron-containing component.

Dosing with conversion α and retention η is described by $m_p = m_x w/(q\alpha\eta)$, where m_x is product mass and w is the Fe_2O_3-equivalent fraction. Compositional analysis after washing closes the balance between the precursor introduced and the material recovered.

Table 2. XRF composition of representative samples

Sample	Fe_2O_3 equiv., wt.%	Other components, wt.%	Calculated matrix, wt.%
PA-52	0.0398	0.5903	99.370
PA-55	8.15	0.7884	91.062
PA-70B	53.1	1.0980	45.802

PA-55 contains 5.71 wt.% total iron. Table 2 shows the transition from a matrix with a small background iron content to a highly filled material. PA-55 retains a predominant calculated polymer fraction and occupies an intermediate filling range. Fe_2O_3 equivalent is used here as the analytical reporting basis for total iron [9].

The amide I band of PA-55 retains the position found in the PA-52 reference. The amide II and amide III bands shift by +0.96 and +1.44 cm^{-1}, respectively. Considered together, these characteristics describe retention of the principal amide spectral profile alongside a change in the local environment of the N-H and C-N groups.

Table 3. Diagnostic infrared band positions, cm^{-1}

Band	PA-52	PA-55	PA-70B
N-H	3307.95	3307.95	3306.02

Band	PA-52	PA-55	PA-70B
Amide I	1643.85	1643.85	1640.95
Amide II	1547.41	1548.37	1550.30

For PA-70B, the amide I displacement relative to PA-52 reaches −2.90 cm^{-1}, while the amide II displacement is +2.89 cm^{-1}. Increased filling therefore accompanies a more pronounced change in the spectral environment of the amide groups. Our processing selection considers filler content together with preservation of the characteristic PA-6 profile [10].

The optical characteristic complements composition and the infrared spectrum. Minimum reflectance is 87.809% at 622 nm for PA-52 and 64.572% at 868 nm for PA-55. The difference between these minima is 23.237 percentage points. PA-70B gives 58.121% at 814 nm. These indicators form part of the spectral record for each sample.

On this basis, we selected PA-55 as the comparatively preferred composition in terms of matrix fraction, amide-band positions and optical response. For the tribological series, composition is specified separately by Fe mass fraction and contact regime. This presentation preserves the physical meaning of each indicator and supports comparison between processing batches.

For PA-6 containing 15 wt.% Fe, linear wear intensity in the water series is 97 μm/km. OTsS-5-5-5 bronze gives 118 μm/km. The calculated reduction in composite wear relative to bronze is 17.8%. In I-50 oil, the comparative effect increases with pressure within the reported series.

Table 4. Comparative linear wear indicators

Medium and regime	PA-6/Fe, μm/km	Bronze, μm/km	Ratio I_h bronze/I_h PA-6/Fe
Water	97	118	1.22
I-50; 2 MPa	1.28	12.50	9.77
I-50; 4 MPa	6.50	502	77.23

The relative reduction was calculated as $\delta = (1 - I_h,c/I_h,b)\cdot 100\%$, where c and b denote composite and bronze. For I-50 oil, the results are 89.76% at 2 MPa and 98.71% at 4 MPa. At 10 MPa, PA-6/Fe gives 25.88 μm/km; intensive wear is recorded for bronze in that regime [11].

For the composite itself, increasing pressure from 2 to 4 MPa raises I_h. The reported ratio therefore describes the ranking of two materials within the same regime. It reflects their different responses to contact loading and to the lubricating medium.

For PA-6 containing 15 wt.% Fe, the compiled comparative data give a 2.1–17.2-fold increase in wear resistance and a 1.4–1.9-fold reduction in the friction coefficient relative to the PA-6 reference. Each indicator is associated with its respective contact conditions [12].

In the comparative series at PV = 0.9 MPa·m/s, increasing Fe content to 15 wt.% accompanies lower wear and contact temperature. Wear rises at 17.5 wt.%. For this series, the region around 15 wt.% corresponds to the wear minimum associated with the sliding conditions.

Analysis of abrasive action gives a different concentration extremum. Figure 1 presents the abrasion-resistance index K_i for the reference material and three filled compositions. The maximum value occurs at 30 wt.% Fe.

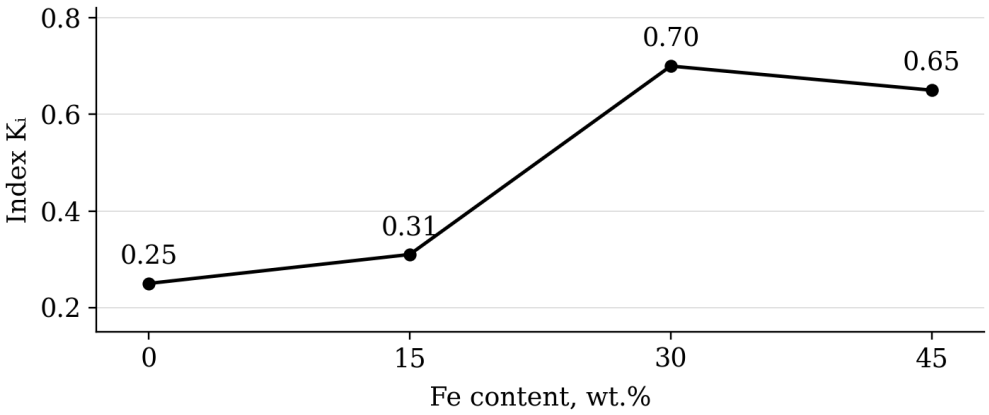

Figure 1. Abrasion-resistance index of PA-6/Fe from comparative data

Discussion

We associate the difference between the extrema with the way the surface layer is damaged. During sliding, PA-6 deformation and transfer-layer formation are significant; under abrasion, resistance to microscratching and retention of solid centres become more influential. In our interpretation model, interfacial bonding transfers load, while detached particle clusters contribute to third-body formation [13].

We select Fe content against the criterion of the particular contact, considering concentration, environment and damage indicator together. Each extremum characterises its respective mechanism of composite operation.

We describe the physical link between friction and thermal loading by the nominal power density $q_n = \mu pv$, where p is contact pressure and v is sliding speed. With p expressed in pascals, q_n has units of W/m^2. This relationship combines mechanical loading with energy generation in the surface layer. Load transfer between the matrix and solid centres forms part of our interpretation of wear [14].

Process control is organised around the condition of the finished product. XRF links dosing to retention of the iron-containing component after washing. The infrared spectrum reflects the state of amide groups following thermal treatment. Reflectance adds a functional characteristic to the batch record. Equal samples taken from the upper, middle and lower reactor zones allow these features to be compared throughout the material volume [15].

Conclusion

An improved PA-6 preparation sequence using $Fe(CH_3COO)_2$ integrates staged dosing, thermal conversion in an oil medium, mixing, rapid cooling and cleaning. Control of these operations is linked to final composition and the spectral state of the product. PA-55 combines 8.15 wt.% Fe_2O_3 equivalent, a 91.062 wt.% calculated matrix fraction and a retained amide I position. This composition serves as a reference for reproducing the structural and spectral characteristics of the material. Our comparative analysis of PA-6/Fe shows that its advantage over bronze depends on environment and pressure. The sliding-wear minimum and the abrasion-resistance maximum belong to different concentration ranges. Composition selection for bushings and guides should therefore be linked to the damage mechanism and the operating regime of the component.

References

[1] G. Czel, A. Sycheva, and D. Janovszky, 'Effect of different fillers on thermal conductivity, tribological properties of Polyamide 6', *Sci. Rep.*, vol. 13, p. 845, 2023, doi: 10.1038/s41598-023-27740-y.

[2] A. N. Sinitsin and V. V. Zuev, 'Effect of fulleroid materials on the mechanical and

tribological properties and dielectric relaxation of polyamide 6 nanocomposites', *Polym. Adv. Technol.*, vol. 28, no. 8, pp. 986–993, 2017, doi: 10.1002/pat.3773.
[3] R. Gupta *et al.*, 'Effect of oleic acid coating of iron oxide nanoparticles on properties of magnetic polyamide-6 nanocomposite', *JOM*, vol. 71, pp. 3119–3128, 2019, doi: 10.1007/s11837-019-03622-5.
[4] A. Dey, M. Zubko, J. Kusz, V. Raghavendra Reddy, and A. Bhattacharjee, 'Effect of reaction protocol on the nature and size of iron oxide nano particles obtained through solventless synthesis using iron(II)acetate: Structural, magnetic and morphological studies', *SN Appl. Sci.*, vol. 2, p. 193, 2020, doi: 10.1007/s42452-019-1881-6.
[5] Z. Man, H. Wang, Q. He, D.-E. Kim, and L. Chang, 'Friction and wear behaviour of additively manufactured continuous carbon fibre reinforced PA6 composites', *Compos. Part B Eng.*, vol. 226, p. 109332, 2021, doi: 10.1016/j.compositesb.2021.109332.
[6] M. García, M. de Rooij, L. Winnubst, W. E. van Zyl, and H. Verweij, 'Friction and wear studies on nylon-6/SiO2 nanocomposites', *J. Appl. Polym. Sci.*, vol. 92, no. 3, pp. 1855–1862, 2004, doi: 10.1002/app.20167.
[7] 'Improvement of dry sliding tribological properties of polyamide 6 using diamond nanoparticles', *Tribol. Int.*, vol. 115, pp. 370–377, 2017, doi: 10.1016/j.triboint.2017.06.003.
[8] Y. L. You, D. X. Li, G. J. Si, and X. Deng, 'Investigation of the influence of solid lubricants on the tribological properties of polyamide 6 nanocomposite', *Wear*, vol. 311, no. 1–2, pp. 57–64, 2014, doi: 10.1016/j.wear.2013.12.018.
[9] S. Savas, H. Pecenek, L. Atabek Savaş, and M. Dogan, 'Mechanical and tribological performances of ceramic microsphere reinforced polyamide 6 composites', *J. Reinf. Plast. Compos.*, vol. 43, no. 15–16, pp. 889–896, 2024, doi: 10.1177/07316844231197257.
[10] S. Musić, M. Ristić, and S. Popović, 'Mössbauer spectroscopic and X-ray diffraction study of the thermal decomposition of Fe(CH3COO)2 and FeOH(CH3COO)2', *J. Radioanal. Nucl. Chem.*, vol. 121, pp. 61–71, 1988, doi: 10.1007/BF02041447.
[11] R. Mohsenzadeh *et al.*, 'Quantitative analysis of tribological performance in polyamide 6/nano-zeolite composites for prosthetic and orthotic applications: Integration of computer vision, numerical modeling, and experimental evaluation', *Tribol. Int.*, vol. 204, p. 110455, 2025, doi: 10.1016/j.triboint.2024.110455.
[12] T. S. Ghanta, S. Aparna, N. Verma, and D. Purnima, 'Review on nano-and microfiller-based polyamide 6 hybrid composite: Effect on mechanical properties and morphology', *Polym. Eng. Sci.*, vol. 60, pp. 1717–1759, 2020, doi: 10.1002/pen.25447.
[13] G. Tang, W. Huang, D. Chang, W. Nie, W. Mi, and W. Yan, 'The friction and wear of aramid fiber-reinforced polyamide 6 composites filled with nano-MoS2', *Polym.-Plast. Technol. Eng.*, vol. 50, no. 15, pp. 1537–1540, 2011, doi: 10.1080/03602559.2011.603779.
[14] 'Tribological behavior of polyamide-6 plastics and their potential use in industrial applications', *Wear*, vol. 376–377, pp. 1391–1398, 2017, doi: 10.1016/j.wear.2017.01.090.
[15] L. Li and G. Yang, 'Variable-temperature FTIR studies on thermal stability of hydrogen bonding in nylon 6/mesoporous silica nanocomposite', *Polym. Int.*, vol. 58, no. 5, pp. 503–510, 2009, doi: 10.1002/pi.2559.